Indian Journal of Chemistry
Vol. 63, July 2024, pp. 685-691
DOI: 10.56042/ijc.v63i7.7550

Effective photocatalytic and solid acid catalytic behaviour of novel bismuth oxy chloride nanomaterial

S Thillainatarajan[a], S Gunasunder[a], I Muthuvel[a,b], T Rajachandrasekar[a], G Thirunarayanan[b], R Vijayalakshmi[c], C Surya[d] & S Sivaselvan*[e]

[a] Photocatalysis Laboratory, Department of Chemistry, M.R. Government Arts College (Affiliated to Bharathidasan University) Mannargudi 614 001, Tamil Nadu, India

[b] Advanced Photocatalysis Laboratory, Department of Chemistry, Annamalai University, Annamalainagar 608 002, Tamil Nadu, India

[c] Department of Petroleum Engineering, Dhaanish Ahmed College of Engineering, Padappai, Chennai 601 301, Tamil Nadu, India

[d] Department of Biochemistry, Dhanalakshmi Srinivasan College of Arts and Science for Women (Autonomous), Perambalur 621 212, Tamil Nadu, India

[e] Department of Physics, M.R. Government Arts College (Affiliated to Bharathidasan University), Mannargudi 614 001, Tamil Nadu, India

E-mail: sivaselvan@mrgac.ac.in, profsivaselvanphy@gmail.com

Received 26 December 2023; accepted (revised) 27 June 2024

In this article, superior photoactive BiOCl nanomaterial has been successfully synthesized and characterized by FT-IR, XRD, SEM, EDS, ECM and UV-DRS analysis respectively. The XRD results show that BiOCl is in tetragonal primitive crystal structure with size of 67 nm. The synthesized BiOCl nanomaterial has been employed as a catalyst to remove methyl orange from aqueous solutions by varying the operational parameters such as *p*H, catalyst concentration, and reusability using photocatalytic method. The maximum degradation of dye that has been attained is 97% under the optimum conditions of *p*H 6 and 1.4 g L^{-1} catalyst concentration. Besides, their removal efficiencies are not much lowered even after five repeated cycles. Moreover, BiOCl nanocatalyst has been used as a solid acid catalyst for the effective synthesis of some chalcones. Hence, the synthesized nanocatalyst could be applied for tertiary process in pilot scale in continuous mode for the treatment of wastewater.

Keywords: Photocatalyst, BiOCl nanocatalyst, Solid acid catalyst, Methyl orange, Wastewater

Water Pollution is one of the most uncontrollable problems that threaten our survival. Among the water contaminants, textile effluents containing dyestuff is considered as the notorious contaminants due to their high industry output, toxicity and non-biodegradability[1]. Recent researchers have worked on the area which is related to environmental problem on toxic wastewater especially in industrial effluent containing organic dyes. More than 50% of textile dyes are azo dyes, such as Methyl Orange (MO), acid orange 7, acid red, reactive blue etc[2,3]. Of the total world dye production, up to 80% is utilized during industrial processing, causing environment pollution resulting in the contribution of aquatic eutrophication[4]. When these effluents enter the aquatic ecosystems, it causes serious environmental and human health problems such as kidney damage, cardiovascular problems, respiratory and renal failure, and digestion problems since dye pollutants are highly toxic and carcinogenic[5-9]. Besides, the workers who handle dyes can have itching in the skin and eyes, rhinitis, occupational asthma or other allergic reactions.

Numerous techniques including adsorption[10], biodegradation and advanced oxidation processes (AOPs), have been tested for dye removal from wastewater[11]. AOP assisted heterogeneous photocatalysis is considered as an effective water remediation technology and the use of semiconductor materials (commonly metallic oxides) as photocatalysts that are activated by irradiation of photons with adequate energy content (ultraviolet or visible light) to generate electrons and holes[12] and then produce highly oxidizing radicals, such as a free hydroxyl radical ($^{\bullet}OH$), responsible for the degradation of organic dyes[13-17]. Different types of photocatalysts have been extensively studied in solution-based dye degradation such as metal oxides (TiO_2 and ZnO), metals, carbon-based nanostructures, and semiconducting materials

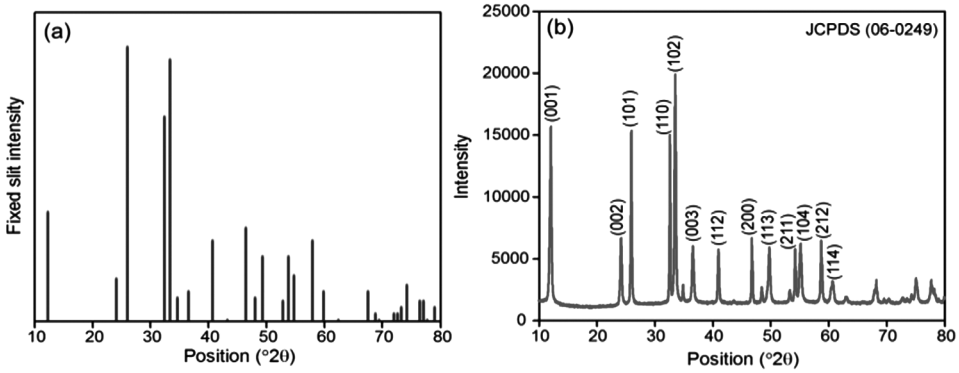

Fig. 1 — XRD patterns of a) standard BiOCl and b) synthesized BiOCl.

based on polymer graphite carbon nitride (g-C_3N_4)[18-20]. The commonly used photocatalyst is titanium dioxide (TiO_2) due to its excellent chemical stability under UV light and high photocatalytic activity. However, it is limited owing to their low photo activation under visible light and high recombination charge rate [21-24]. In recent years, bismuth-based photocatalysts has been reported as an effective for dye degradation under sunlight[25,26]. Its unique properties depend on size and morphology, as well as the basic building block structures, including synthesized nanosheets[27-29], nanotubes[30,31] and nanowires[32]. They have a better photocatalytic activity of organic dye degradation than TiO_2 Degussa P25[33].

In this present work, BiOCl nanoparticles were fabricated using the sol-gel method using $Bi(NO_3)_3.5H_2O$ as source of bismuth. The synthesized nanoparticles were then systematically examined by various analytical and spectroscopic tools. The impact of the process parameters such as *p*H of the initial dye solution, the amount of BiOCl and the initial concentration of the dye, on dye removal efficiency was studied and optimized. Furthermore, synthesized BiOCl nanoparticle was reused several times in order to evaluate their stability. The BiOCl samples had superior catalytic activities toward methyl orange (MO) degradation under ultraviolet (UV) irradiation.

Results and Discussion

Characterization of BiOCl nanomaterials

X-Ray diffraction (Fig. 1a) shows the BiOCl standard XRD pattern and BiOCl (Fig. 1b) was prepared. The tetragonal primitive crystal structure is clearly revealed. All the planes coincide well with BiOCl's standard JCPDS file (No. 06-0249, a = 3.891 Å, c = 7.369 Å)[34]. It was observed that this pattern has no peaks for impurity.

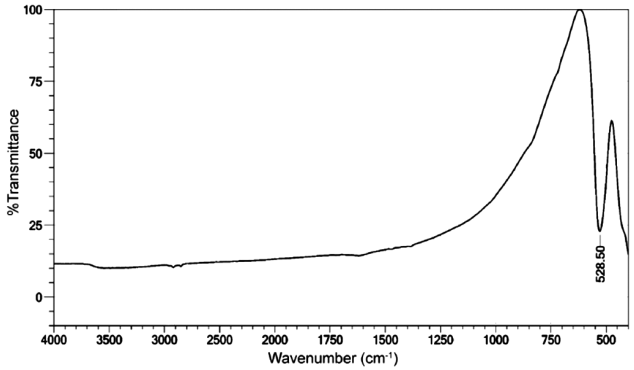

Fig. 2 — FT-IR spectrum of prepared BiOCl sample.

Thus, the synthesized powder is well crystallized with a high purity in BiOCl. FT-IR spectrum of prepared BiOCl sample is shown in Fig. 2.

Fig. 2 shows that the strong peak at low frequency about 528 cm^{-1} was attributed to the Bi–O vibration of chemical bonds in BiOCl[35]. SEM images of prepared BiOCl are shown in Fig. 3a-c revealing the morphology and composition of BiOCl powder. EDX coupled with ECM. It is clearly shown that the products are composed of homogeneous well-defined particles from low magnification images (Fig. 3a and b). Higher magnification image (Fig. 3c) shows that particles consist of plate like structure with thickness of 80 nm. The presence of the elements Bi, O, Cl in the catalyst are confirmed by EDX analysis from the particular selected area (Fig. 3d). The EDX analysis revealed that the relative atoms are present in the prepared sample. To confirm the presence of these elements BiOCl was analyzed by elemental mapping (Fig. 3d inset).The different colour areas indicate that the enriched areas of the Bi, O and Cl. UV-Diffused reflectance spectrum of prepared BiOCl was shown in Fig. 4.

The BiOCl sample exhibited absorption in the UV light region and the absorption edge was located at

about 364 nm. The band gap energy (E_g value) of the BiOCl sample could be thus estimated from Tauc plot of KM *versus* photon energy (hν). The intercept of the tangent to the x-axis will give a good approximation of the band gap energy for the BiOCl powder[36]. Tauc plot of KM *versus* photon energy (hν) of BiOCl powder is shown in Fig. 4a. The E_g estimated from the intercept of the tangent to the plot was 3.53 eV.

Effect of process parameters on MO degradation with BiOCl

Effect of catalyst loading

The analysis of degradation rate with different amounts of catalyst is necessary to find out the minimum amount of catalyst required for the removal of dye from the aqueous solution. Therefore, optimization of the catalyst dose is required to effectively mineralize MO. The experiment was conducted under UV-A light irradiation with a varying catalyst concentration from 0.6 to 1.8 g L^{-1} in aqueous MO solution. The degradation rate increases from 0.023 to 0.0776 min^{-1} with an increase of catalyst weight ranging from 0.6 to 1.4 g L^{-1} at 20 min (Fig. 5). The rate constant is suddenly decreased by further increase of the catalyst amount (above 1.4 g L^{-1}). The decrease in efficiency of MO at higher amount (above 1.4 g L^{-1}) is caused by the light reflectance of catalyst particles[37,38]. Thus the optimum amount of catalyst for efficient degradation of MO is considered as 1.4 g L^{-1}.

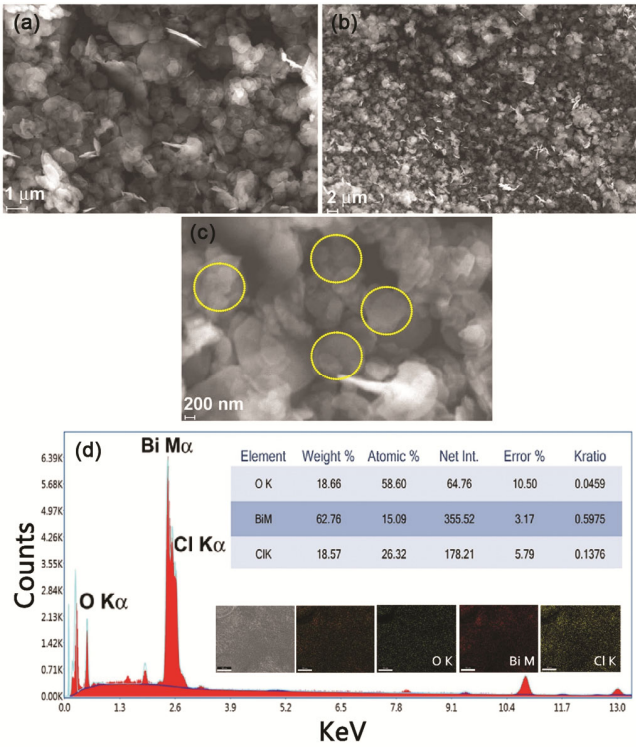

Fig. 3 — SEM images of BiOCl: a) 1 µm, b) 2 µm and c) 200 nm d) EDX image of BiOCl and inset of colour mapping images of BiOCl

Influence of initial solution *p*H

The influence of *p*H on MO degradation (Fig. 6) was studied from 4 to 9. At *p*H 6 the maximum 99 percent degradation percentage was observed (60 min). Above *p*H 6 the effectiveness of degradation decreases. Because of the dissolution of BiOCl, the removal efficiency is less at low *p*H. The effectiveness of a catalyst's degradation depends on the adsorption of the dye molecules.

The percentages of *p*H 4, 5, 6, 7 and 9 adsorption were found to be at equilibrium of 10.9, 12.6, 18.8, 15.7 and 13.5 respectively. Due to the maximum adsorption at *p*H 6, the degradation at this *p*H is high. At *p*H above 6, the catalyst surface is negatively charged and the electrostatic attraction between the dye anion and the negatively charged catalyst becomes weak, resulting in the reduction of degradation rate[37-39]. Hence, *p*H 6 is recommended optimum *p*H for MO mineralisation.

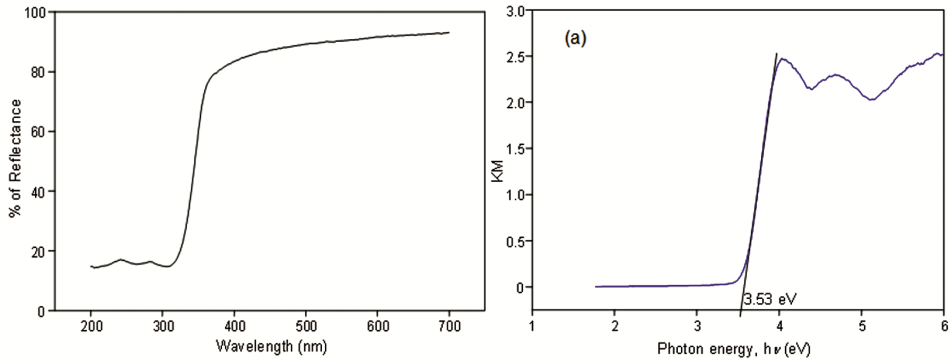

Fig. 4 — UV-DRS of BiOCl a) KM of BiOCl

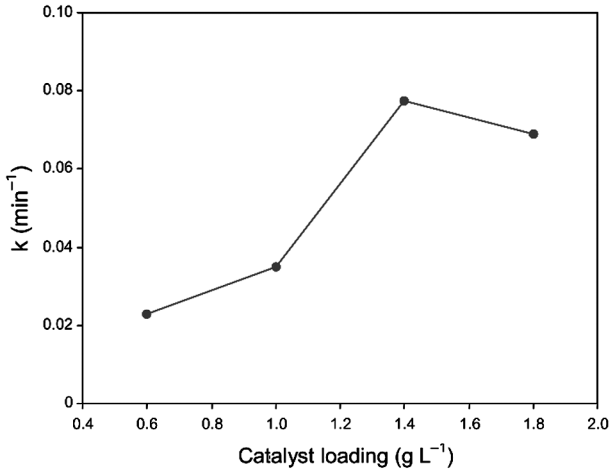

Fig. 5 — Effect of catalyst loading (UV)[MO] = 3×10^{-4} M, airflow rate = 8.1 mL s^{-1}, *p*H = 6, irradiation time = 20 min.

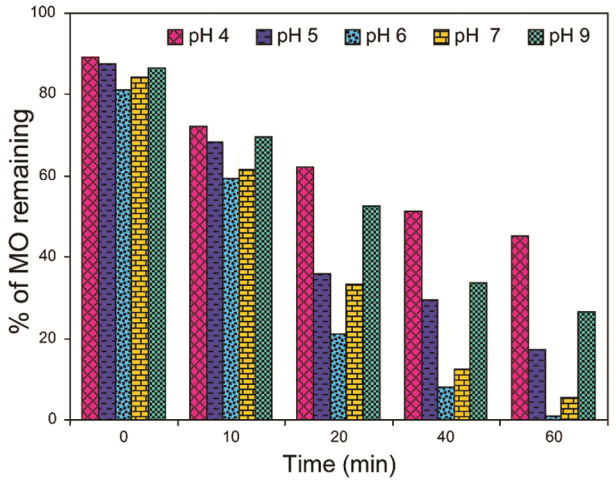

Fig. 6 — Effect of initial solution *p*H (UV) [MO] = 3×10^{-4} M, catalyst suspended = 1.4g L^{-1}, airflow rate = 8.1 mL s^{-1}

Effect of Initial Dye Concentration

Dye concentration is an important parameter in wastewater treatment. The effect of initial dye concentration of MO on degradation was investigated over the concentration of 1 to 5 × 10^{-4} M. Increasing the initial dye concentration from 1 to 5×10^{-4}M decreases the degradation rate constant from 0.1606 to 0.0537 min^{-1} (Fig. 7) at the time of 20 min. The catalyst amount and UV power remains same in all the experiments. The generation of hydroxyl radical remains constant. The rate of degradation is related to the •OH radical formation on catalyst surface and probability of •OH radical reacting with dye molecule. When the initial concentration of the dye increases, the path length of photon entering into the solution and the photocatalytic degradation efficiency were decreased[37,38].

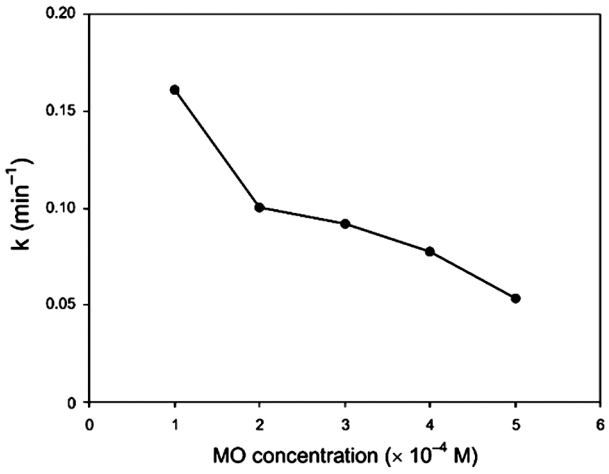

Fig. 7 — Effect of initial dye concentration (UV). Catalyst suspended = 1.4 g L^{-1}, Air flow rate = 8.1 mL s^{-1}, *p*H = 6, irradiation time = 20 min.

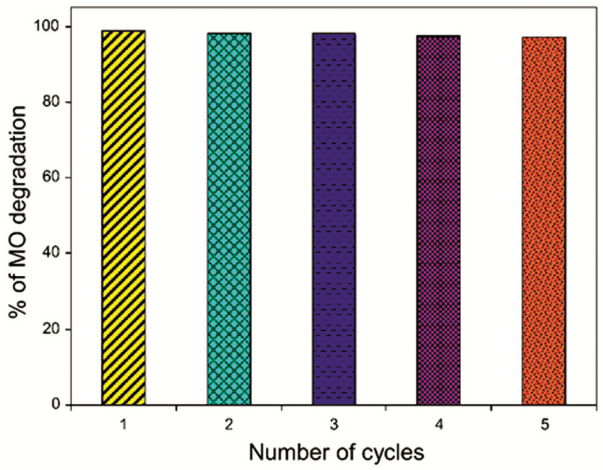

Fig. 8 — Long-term stability (UV). [MO] = 3×10^{-4} M, catalyst suspended = 1.4 g L^{-1}, airflow rate = 8.1 mL s^{-1}, *p*H = 6.

Long-term stability

The results of catalyst recyclability are indicated in Fig. 8. The catalyst was recovered and reused five times in order to check the efficiency of synthesized BiOCl under identical reaction conditions. The results revealed that BiOCl exhibited an excellent photostability and sustained their degradation ability (97%) even after five cycles. This makes the catalyst apt for continuous wastewater treatment.

BiOCl Photocatalytic mechanism

By means of a photocatalytic reaction involving photogenerated electrons and holes and reactive oxygen species, degradation of harmful organic contaminants in water can be degraded or mineralized into harmless /inoffensive products (CO_2 and H_2O).

Photodegradation of organic contaminants by the use of BiOCl nanocatalyst occurs when the photocatalyst absorbs light from the UVA light source with appropriate wavelength. This light energy excites and promotes electrons to their conduction band within the valence band of the photocatalyst. This leads to the creation of positive charges (holes) and negative charges (electrons) on the bands of valence and conduction respectively, leading to the creation of pairs of electron-hole. The hole oxidizes water molecule into hydrogen gas and hydroxyl radical while the electron reduces oxygen molecules into superoxide radical. The hydroxyl and superoxide radicals then attack and degrade the pollutants into harmless products[37,38]. The photodegradation process mechanism is depicted in Fig. 9.

$HO_2^{\bullet}$ can lead to the formation of H_2O_2:

$$O_2 + e^- \rightarrow O_2^{\bullet-} \quad \ldots (1)$$

$$O_2^{\bullet-} + H^+ \rightarrow HO_2^{\bullet} \quad \ldots (2)$$

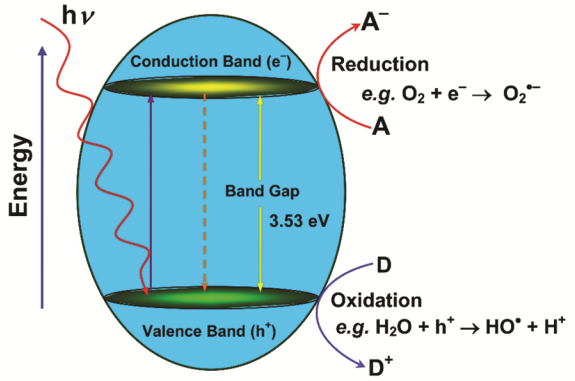

Fig. 9 — Schematic representation of BiOCl nanocatalyst mechanism of dye degradation

$$HO_2^{\bullet} + e^- \rightarrow HO_2^- \quad \ldots (3)$$

$$HO_2^- + H^+ \rightarrow H_2O_2 \quad \ldots (4)$$

Photogenerated holes can react with adsorbed water molecules (or hydroxide anions) to give hydroxyl radicals:

$$H_2O + h^+ \rightarrow HO^{\bullet} + H^+ \quad \ldots (5)$$

Synthesis of Chalcones

An appropriate mixture of aryl methyl ketones (100mmol) and substituted benzaldehydes (100mmol) were mixed thoroughly with 1.5mL of methanol in a 50 mL corning beaker for attaining homogeneity. Then, 0.05 g of BiOCl catalyst were added in the mixture and closed the beaker with lid. The reaction mixture was subjected to heat in a microwave oven (Samsung, Grill GW73BD Model, 100–750 W, 2450 MHz, 230 A/c) at 650W for 3–5 m in the period of 30 second (Scheme1). After complete conversion of the ketones as monitored by TLC, the mixture was allowed to stand for 20 minutes. The reaction product mixture was extracted with 10 mL of dichloromethane and the catalyst was removed by simple filtration. Evaporation of dichloromethane contributed to a crude product. Further this was recrystallized with ethanol. The purities of synthesized enones were examined by their physical constants. The catalyst was washed with ethyl acetate (5 mL) and heated on an oven at 110°C for 5 h. Afterwards, this catalyst was reused for this reaction as second time. But unfortunately, this catalyst does not catalyze this condensation. Therefore, this catalyst was not reusable. This synthetic protocol was used for synthesis of some

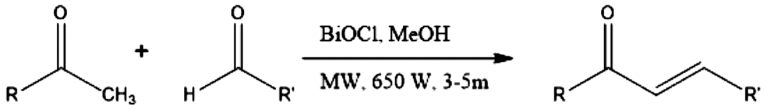

Entry	R	R'	Yield (%)	Time (m)	m.p. (°C)
1	Phenyl	Phenyl	95	3.5	56–57 (55–58)[40]
2	Phenyl	4-Methoxyphenyl	97	4	165–166 (164)[40]
3	1-Naphthyl	Phenyl	92	5	101–102(100–102)[40]
4	2-Naphthyl	Phenyl	96	4.5	105–106(104–105)[40]
5	3-Cyanophenyl	Phenyl	93	3.5	134-135(133–135)[41]
6	2-Pyrenyl	Phenyl	95	3.5	162–163(161–162)[42]
7	Phenyl	1-Pyrenyl	97	4	177–178(176–177)[43]
8	3,4-Dimethoxyphenyl	Phenyl	98	3.5	74–75(75-76)[44]
9	2,5-Dimethylthiazole	Phenyl	97	3	60–61(61-62)[45]
10	4-Piperidiniphenyl	Phenyl	97	3.5	191-192(192-193)[46]

Scheme 1 — Synthesis of chalcones by BiOClcatalyzed microwave assisted method.

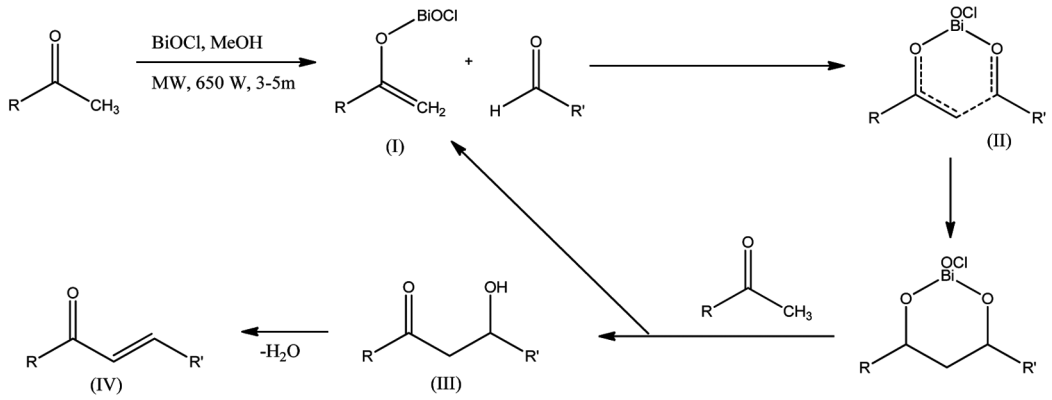

Fig. 10 — Proposed general mechanism for the synthesis of enones by BiOCl catalyzed aldol condensation.

enones with their physical constants and reaction times are given in Scheme 1.

This condensation reaction was proceeded with *in situ* BiOCl catalyzed crossed aldol method. The proposed general mechanism of this reaction is given in Fig. 10. Aryl methyl ketones approached bismuth oxy chloride and enolization occur (I). The enol form aryl ketone with catalyst reacts with aryl aldehydes to form the cyclic intermediate (II). This intermediate again approach the aryl methyl ketone to form enol with catalyst (I) and β-hydroxy aryl ketone (III). Elimination of water from β-hydroxy aryl ketone afforded the desired enone (IV).

Experimental Section

Materials and Methods

Methyl Orange dye (MO) (C.I-13025), bismuth nitrate pentahydrate (Qualigens), potassium chloride (Qualigens), acetic acid, NaOH, H_2SO_4 from (Himedia Chemicals) were commercially procured and used for the research work. Ferrous ammonium sulfate, AnalaR silver sulfate (Himedia), mercury(II) sulfate (Merck 90%), potassium dichromate, ferroin indicator (Sd fine) solutions were used for chemical oxygen demand analysis. The experimental solution was prepared using distilled water.

Synthesis of BiOCl nanostructures

In a typical synthesis, 0.01 mol of KCl was dissolved in 100 mL of H_2O, and 0.01 mol of $Bi(NO_3)_3{\cdot}5H_2O$ was dissolved in 100 mL of an aqueous solution containing 9 mL of acetic acid and vigorously stirred for 30 min. The $Bi(NO_3)_3$ solution was added drop wise into the KCl solution and stirred magnetically for 1 h at room temperature. The resulting suspension was aged for 4 h. The precipitate (BiOCl) was collected by filtration, washed thoroughly four times with distilled water and ethanol, and then dried at 60°C overnight to get the final product of BiOCl.

Photodegradation experiments and characterization techniques

Heber multilamp photo reactor model HML-MP 88 was utilized for photodegradation. The details of the photo reactor and photocatalytic experiment with 50 mL of dye solution and appropriate quantity of photocatalyst under UV-A light (365 nm) irradiation was reported earlier[37]. Characterization by FT-IR, XRD,SEM-EDX, ECM and UV-DRS has already been given earlier[38,47]. COD was determined using the literature procedure[48].

Conclusion

A simple and cost-effective BiOCl nanomaterials was fabricated successfully and characterized by XRD, FTIR, SEM-EDS with ECM and UV-DRS. XRD analysis revealed that the presence of tetragonal primitive crystal structure that was confirmed by JCPDS card no. 06-0249. The FTIR analysis confirmed the presence of Bi-O stretching vibrations. Higher magnification image showed that the particles having a plate like structure with thickness of 80 nm. The presence of the elements Bi, O, Cl in the catalyst were confirmed by EDX analysis and further confirmed by elemental colour mapping. The BiOCl sample exhibited absorption in the UV light region and the absorption edge was located at about 364 nm. By applying KM function, the E_g estimated band gap was 3.53 eV. In the presence of BiOCl, optimum *p*H and catalyst concentration for MO mineralization with UV-light were found to be *p*H 6 and 1.4 g L^{-1}, respectively. The increase in dye concentration decreases the removal rate. In reusability of BiOCl

analysis, almost 97% of degradation was observed for all the five cycles. Hence the BiOCl catalyst was found to be reusable for industrial applications. Moreover, BiOCl nanocatalyst was effective solid acidic catalyst for the synthesis of chalcones in a greener way.

Acknowledgment

One of the authors (I. Muthuvel) thanks financial support from the University Grants Commission (UGC), New Delhi, for research grant No. UGC sanctioned letter F.No-43-222/2014(SR). S. Sivaselvan thanks the International research center, Kalasalingam academy of research and education, Kalasalingam University, Krishnankoil-626 126, Tamilnadu, India for taking SEM-EDS and ECM analysis.

References

1 Aljerf L, *J Env Manage*, 225 (2018) 120.
2 Xu S S, HeL Z, Ying H, Chen J, Xiao X & Yan B, *J Hazard Mater*, 152 (2008) 1301.
3 Lee J W, Choi S P, Thiruvenkatachari R, Shim W G & Moon H, *Dyes Pigm*, 69 (2006) 196.
4 Konstantinou I K &Albanis T A, *Appl Catal B: Env*, 49 (2004) 1.
5 Sen S K, Raut S, Bandyopadhyay P & Raut S, *Fung Bio Rev,* 30 (2016) 112.
6 Miranda R D C, Gomes E D B, Pereira N J, Marin-Morales M A, Machado K M & Gusmao N B, *Biores Tech*, 142 (2013) 361.
7 Muthuvel I, Sathyapriya S, Suguna S, Gowthami K, Thirunarayanan G, Rajalakshmi S, Sundaramurthy N, Dinesh Karthik A & Rajachandrasekar T, *Mater Today Proc*, 43 (2021) 2274.
8 Cotillas S, Clematis D, Canizares P, Carpanese M P, Rodrigo M A & Panizza M, *Chemosphere,* 199 (2018) 445.
9 Chatterjee D, Patnam V R, Sikdar A, Joshi P, Misra R & Rao N N, *J Hazard Mater,* 156 (2008) 435.
10 Dong S, Xia L, Guo T, Zhang F, Cui L, Su D, Wang X & Guo W, *J Sun Appl Surf Sci*, 445 (2018) 30.
11 Dong S, Cui L, Zhang W, Xia L, Zhou S, Russell C K, Fan M, Feng J & Sun J, *Chem Eng J,* 384 (2020) 273.
12 Ren H, Koshy P, ChenW F, Qi S & Sorrell C C, *J Hazard Mater,* 325 (2017) 340.
13 Asghar A, Raman A A A & Daud W M A.W, *J Clean Prod,* 87 (2015) 826.
14 Wetchakun K, Wetchakun N & Sakulsermsuk S, *J Indian Engg Chem,*71 (2019) 19.
15 Al-Mamun M R, Kader S, Islam M S & Khan M Z H, *J Env Chem Eng,* 7 (2019) 103248.
16 Nguyen C H, Fu C C & Juang R S, *J Clean Prod*, 202 (2018) 413.
17 Shaban Y A, *Arab J Chem*, 12 (2019) 652.
18 Pawar R C, Kang S, Park J H, Kim J H, Ahn S & Lee CS*, Sci Rep*, 61 (2016) 14.
19 Anwer H, Mahmood A, LeeKim J, K H, Park J W &Yip A C K, *Nano Res,*12 (2019) 955.
20 Tan L, Yu C, Wang M, Zhang S, Sun J, Dong S & Sun J, *Appl Surf Sci,* 467 (2019) 286.
21 Markad G B, Kapoor S, Haram S K & Thakur P, *Sol Energy*, 144 (2017)127.
22 Wanag A, Kusiak-Nejman E, Kowalczyk Ł, Kapica-Kozar J, Ohtani B & Morawski A W, *Appl Surf Sci,* 437 (2018) 441.
23 Ni Z, Sun Y, Zhang Y & Dong F, *Appl Surf Sci,* 365 (2016) 314.
24 Cao X, Tao J, Xiao X & Nan J, *J Photochem Photobio: A Chem*, 364 (2018) 202).
25 He R, Cao S, Zhou P & Yu J, *Chin J Cat*, 35 (2014) 989.
26 Meng X & Zhang Z, *J Mol Catal Chem*, 423 (2016) 533.
27 Wang C, Zhang X, Yuan B, Shao C & Liu Y, *Micro Nano Lett,* 7 (2012)152.
28 Li K, Liang Y, Yang J, Gao Q, Zhu Y, Liu S, Xu R & Wu X, *J Alloy Comp,* 695 (2017) 238.
29 Song Z, Dong X, Fang J, Xiong C, Wang N & Tang X, *J Hazard Mater,* 377 (2019) 371.
30 Deng H, Wang J, Peng Q, Wang X & Li Y, *Chem Eur J*, 11 (2005) 6519.
31 Zhao S, Liu T, Zheng S, Zeng W, Li T, Zhang Y, Hussain S, Hou D & Peng X, *Mater Lett*, 168 (2016) 13.
32 Wu S, Wang C, Cui Y, Wang T, Huang B, Zhang X & Qin X P, *Brault Mater Lett,* 64 (2010) 115.
33 Song J, Fan Q, Zhu W, Wang R & Dong Z, *Mater Lett,* 165 (2016) 14.
34 Shi Z O, Wang Y, Fan C M, Wang Y F & Ding G Y*, Trans Nonfer Met Soc Chin*, 21 (2011) 2254.
35 Bai Y, Wang Y Q, Liu J Y & Liu X J, *RSC Adv,* 4 (2014) 19456.
36 Man H, Wang C, Sun Y, Ning Y, Song P & Huang W*, J Materiomics,* 2 (2016) 338.
37 Suppuraj P, Thirumalai K, Parthiban S, Swaminathan M & Muthuvel I, *Nanosci Nanotech*, 20 (2020) 709.
38 Gowthami K, Suppuraj P, Thirunarayanan G, Krishnakumar B, Sobral A J F N, Swaminathan M & Muthuvel I, *Iran Chem Comm*, 6 (2018) 97.
39 Bolobajev J, Trapido M & Goi A, *Chemosphere* 153 (2016) 220.
40 Thirunarayanan G, Mayavel P & Thirumurthy K, *Spectrochim Acta*, 91A (2012) 18.
41 Kamalakkannan D, Senbagam R, Vanangamudi G & Thirunarayanan G, *J Mol Struct,* 1264 (2022) 133218.
42 Muthuvel I, Thirunarayanan G, Thangaraj V, Sundaramurthy N, Rajalakshmi S & Usha V, *Mat Today Proc,* 43 (2021) 2203.
43 Sekar K G, Janaki P, Muthuvel I, Usha V, Thirumurthy K & Thirunarayanan G, *Mat Today Proc,* 43 (2021) 2208.
44 Mala V, Muthuvel I, Thirunarayanan G & Usha V*, Mat Today Proc*, 43 (2021) 2117.
45 Balaji V, Manikandan V, Rajarajan M, Usha V, Rajalakshmi S, Venkatachalam P, Muthuvel I & Thirunarayanan G, *Mat Today Proc*, 22 (2020) 931.
46 Ranganathan K, Kamalakkannan D, Suresh R, Sakthinathan S P, Arulkumaran R, Sundararajan R, Manikandan V & Thirunarayanan G*, Indian J Chem*, 58B (2019) 1131.
47 Muthuvel I, Gowthami K, Thirunarayanan G, Suppuraj P, Krishnakumar B, Sobral A J F N & Swaminathan M, *Int J Ind Chem*, 10 (2019) 77.
48 Muthuvel I & Swaminathan M, *Sol Energy Mater Sol Cells*, 92 (2008) 857.